Triggers of Permo-Triassic boundary mass extinction in South China: The Siberian Traps or Paleo-Tethys ignimbrite flare-up?

Bin He [a], Yu-Ting Zhong [a,b], Yi-Gang Xu [a,*], Xian-Hua Li [c]

[a] *State Key Laboratory of Isotope Geochemistry, Guangzhou Institute of Geochemistry, Chinese Academy of Sciences, Guangzhou 510640, China*
[b] *University of Chinese Academy of Sciences, Beijing 100049, China*
[c] *State Key Laboratory of Lithospheric Evolution, Institute of Geology and Geophysics, Chinese Academy of Sciences, Beijing 100029, China*

ABSTRACT

Assessment of the synchroneity between the Siberian Traps and the Permo-Triassic boundary (PTB) mass extinction has led to the proposition that the Siberian flood volcanism was responsible for the severest biotic crisis in the Phanerozoic. However, recent studies suggest that the Siberian Traps may have postdated the main extinction horizon. In this paper, we demonstrate, using stratigraphy, a time and intensity coincidence between PTB volcanic ash and the main extinction horizon. Geochemistry of the PTB volcanic ashes in five sections in South China indicates that they were derived from continental magmatic arc. Zircons extracted from the PTB volcanic ashes have negative $\varepsilon_{Hf(t)}$ (-12.9 to -2.0) and $\delta^{18}O$ (6.8 to 10.9‰), consistent with an acidic volcanism and a crustal-derived origin, and therefore exclude a genetic link between the PTB mass extinction and the Siberian Traps. On the basis of spatial variation in the number of the PTB volcanic ash layers and the thickness of the ash layers in South China, we propose that the PTB volcanic ash may be related to Paleo-Tethys continental arc magmatism in the Kunlun area. Ignimbrite flare-up related to rapid plate subduction during the final assemblage of the Pangea super-continent may have generated a volcanic winter, which eventually triggered the collapse of ecosystem and ultimately mass extinction at the end of the Permian. The Siberian Traps may have been responsible for a greenhouse effect and so have been responsible for both a second pulse of the extinction event and Early Triassic ecological evolution.

1. Introduction

The Permo-Triassic boundary (PTB) mass extinction was the severest biotic crisis in Phanerozoic, affecting over 90% marine species, 70% land vertebrate genera and most land vegetation (Erwin, 1994). Although no consensus has been reached so far on the causal mechanisms, the ~250 Ma Siberian Traps is widely believed to be the ultimate cause of PTB mass extinction due to the coincidence of these two events (e.g., Campbell et al., 1992; Courtillot, 1994; Courtillot and Renne, 2003; Kamo et al., 2003, 2006; Racki and Wignall, 2005; Reichow et al., 2002; Renne et al., 1995). However, two potential pitfalls are associated with this methodology/reasoning:

(a) If the two events took place at the same time, they are possibly but not necessarily related to each other. In the PTB case, the role of volcanism as the cause of mass extinction is considered important given the presence of numerous volcanic ash layers around the PTB. If this volcanic ash has the same age and composition as those of the Siberian Traps, a consanguineous association between them can thus be established. The PTB volcanic

ash was previously considered to be felsic rather than mafic and be related to plate subduction or a magmatic arc (e.g., Clark et al., 1986; Yang et al., 1991; Yin et al., 1992, 2007; Zhou and Kyte, 1988). Thus, the provenance of the PTB volcanic ash and its genetic relationship related to the Siberian Traps deserve further investigation.

(b) The link between the Siberian Traps and the PTB mass extinction was initially established based on the synchroneity of these two events. However, the dating techniques used in the early studies on PTB (SHRIMP and Ar–Ar dating) generally have the analytical precision of ~1%, which corresponds to an uncertainty of 2–3 Ma (Campbell et al., 1992; Renne et al., 1995). Such an uncertainty is insufficient to constrain the temporal relationship of the PTB and the mass extinction which is believed to have occurred within 0.2 Myr (Shen et al., 2011). A newly developed zircon U–Pb dating technique, chemical abrasion-thermal ionization mass spectrometry (CA-TIMS), can improve the precision up to 0.1% on the analyses for individual zircon grains, and is therefore suitable for the accurate age constraints of PTB (Shen et al., 2011). The CA-TIMS zircon U–Pb ages for the Siberian Traps indicate that the eruption of the flood basalts mainly occurred between 251.7 ± 0.4 and 251.3 ± 0.3 Ma (Kamo et al., 2003), which significantly postdate the main PTB extinction horizon (252.28 ± 0.08 Ma)

(Shen et al., 2011) (Fig. 1). This result is consistent with the observation that the transition from Permian to Triassic fossil assemblages in Russia had started before the eruption of the Siberian Traps (Sadovnikov, 2008). Therefore, the model involving the Siberian Traps as the most significant cause of the PTB mass extinction needs to be re-evaluated.

In this study, we carried out an integrated investigation of geology, mineralogy, whole-rock geochemistry and zircon Hf–O isotopes of the PTB volcanic ash in South China, in order to define the relationship between the volcanic ash and the PTB mass extinction, and to unravel the provenance of volcanic ashes around the PTB. Our results show that (1) the main PTB extinction horizon rests on a layer of volcanic ash, consistent with a causal link between the volcanism and mass extinction, and (2) a crustal origin of the PTB volcanic ash layers, which rules out a genetic link to the Siberian Traps. Finally, we propose that the PTB volcanic ash in South China may be related to ignimbrite flare-up caused by rapid plate subduction during Pangea assembly.

2. Geological background and sampling

The Permian–Triassic boundary Global Stratotype Section and Point (GSSP) was established at D section of Meishan, Changxing, Zhejiang Province in South China (Yin et al., 2001). The well-established stratigraphic columns of a number of the PTB sections in South China show that abundant volcanic ash occurs around PTB (Fig. 2). These ash layers have been extensively studied in the past 30 years (e.g., Bowring et al., 1998; Clark et al., 1986; Metcalfe et al., 1999; Mundil et al., 2001, 2004; Shen et al., 2011, 2012, 2013; Zhou and Kyte, 1988). It is widely accepted that the PTB volcanic ash layers may have been deposited during the latest Permian and the earliest Triassic, and that they are felsic in composition and may have been formed in a subduction-related setting (Clark et al., 1986; Gao et al., 2013; Isozaki et al., 2007; Shen et al., 2012; Yang et al., 2012; Yin et al., 2007; Zhou and Kyte, 1988).

Five typical PTB sections (Meishan, Shangsi, Chaotian, Dongpan and Rencunping) in South China (Fig. 3) are targeted in this study for mineral and whole-rock compositions and zircon Hf–O isotopic analyses. Using our own field observations with those reported in the in
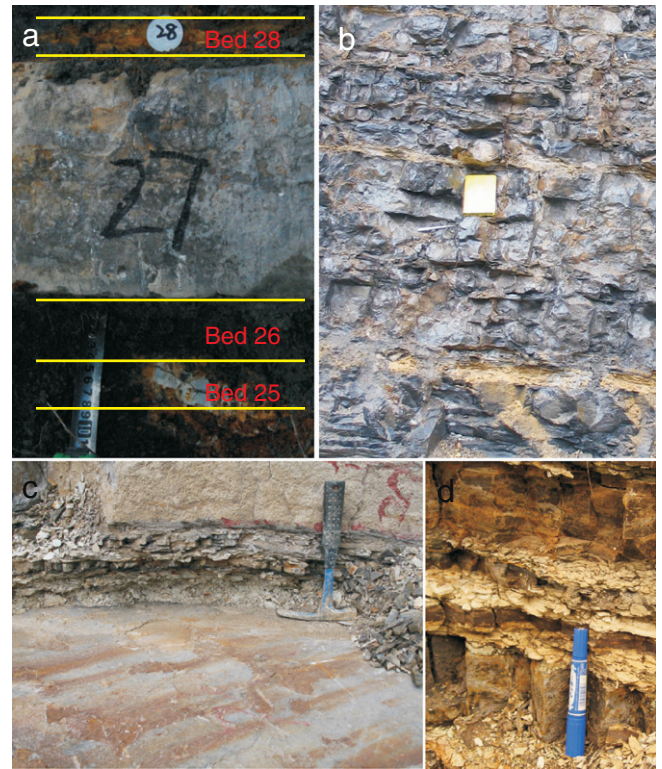

Fig. 2. Field photographs of the PTB volcanic ashes at (a) Meishan, (b) Chaotian, (c) Shangsi, and (d) Dongpan sections. Note: The length of the yellow notebook in (b) is 18 cm.

literature, the main characteristics of the PTB volcanic ash layers in South China are summarized as follows:

(1) Although the presence of abundant volcanic ash is common in all the PTB sections in South China, the numbers of ash layers and
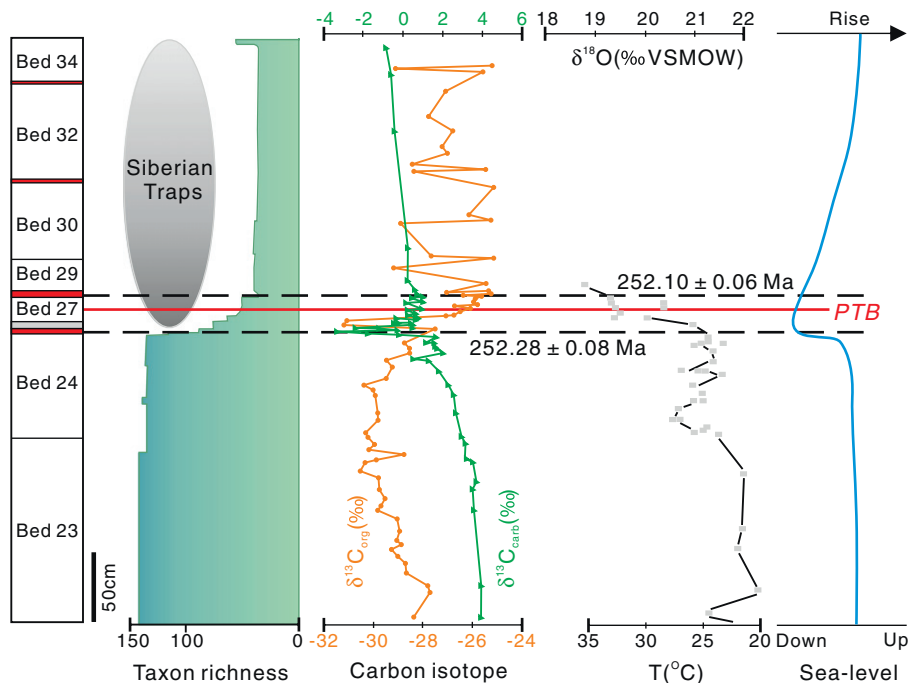

Fig. 1. A chart showing the PTB event sequences at Meishan section. Data sources: Bed numbers are after Yin et al. (2001); age, bio-diversity, $\delta^{13}C_{carb}$ and $\delta^{13}C_{org}$ are after Shen et al. (2011); $\delta^{18}O$ of conodonts and inferred sea-water surface temperature are after Joachimski et al. (2012); and duration of Siberian Traps is after Kamo et al. (2003). PTB = Permo-Triassic boundary.
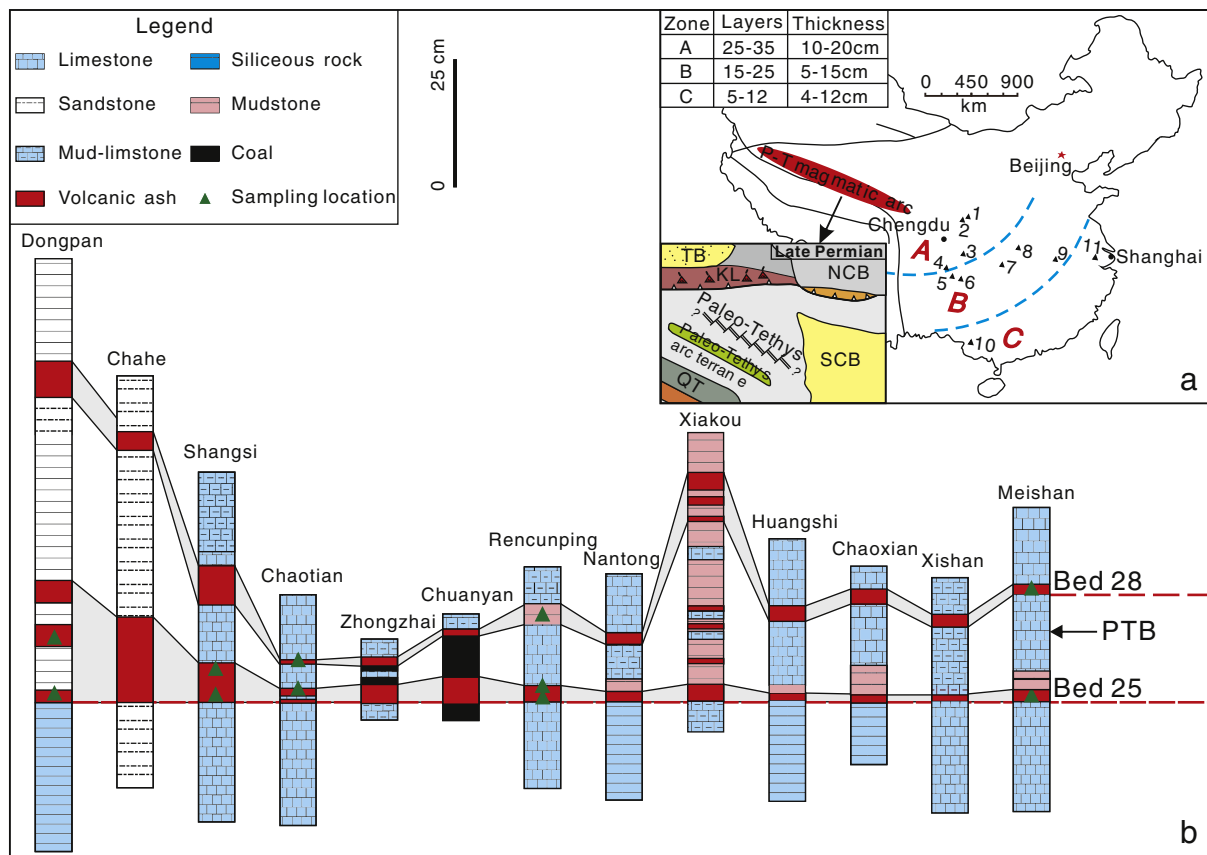
Fig. 3. (a) Location map of sampling sections and (b) stratigraphic correlation of 13 PTB sections in South China. 1 — Chaotian, 2 — Shangsi, 3 — Liangfenya, 4 — Chuanyan, 5 — Zhongzhai, 6 — Chahe, 7 — Rencunping, 8 — Xiakou, 9 — Huangshi, 10 — Dongpan, and 11 — Meishan; Zones A, B and C are divided in terms of the number and total thickness of ash layers, shown in the Table inset. The inset figure shows a continental magmatic arc in the Kunlun area. TB = Tarim Block; KL = Kunlun; NCB = North China Block; SCB = South China Block.

the thickness of each ash layer are highly variable from one section to another (e.g., Gao et al., 2013; Isozaki et al., 2004, 2007; Li et al., 1986; Shen et al., 2012, 2013). In South China, the PTB volcanic ashes are divided into three zones, Zones A, B and C, in terms of the numbers and total thickness of ash layers (Fig. 3a). 25–35 ash layers are present in Zone A in the northwest part of South China with a total thickness varying from 10 to 20 cm in different sections, whereas 15–25 ash layers in Zone B in the central part of South China have a total thickness of 5–15 cm and 5–12 ash layers in Zone C have a total thickness of 4–12 cm. The decrease in the layer number and thickness from Zone A to Zone C indicates that the PTB volcanic ash may have had their provenance in West China.

(2) Two layers of volcanic ash (Beds 25 and 28) in the Meishan GSSP section are exactly on the PTB extinction horizons (Figs. 1 and 3b) (e.g., Shen et al., 2011; Song et al., 2013; Xie et al., 2007; Yin et al., 2007, 2012). Overall Bed 25 and its equivalent layer in other sections are much better correlated than other ash layers around PTB in South China. The 4–20 cm-thick Bed 25 can be found in the same stratigraphic level in all the PTB sections in South China, except in a few sections where Bed 25 was deposited above the storm wave base and the PTB is unconformity.

(3) The CA-TIMS zircon U–Pb dating results for the ash layers in the Meishan and Shangsi sections show that the Late Permian volcanism started at 254.3 Ma and ended at 251.3 Ma, with a main peak at 252.2 Ma (e.g., Bowring et al., 1998; Galfetti et al., 2007; Mundil et al., 2004; Shen et al., 2011).

(4) As revealed by the temporal variation in the thickness of the ash layers from Zone A to Zone C (Fig. 3), the volcanism intensified during the Changsingian and reached its climax in the latest

Permian. The ash layers were initially thought to represent regional eruptive activity associated with a volcanic arc along the margin of the South China craton (Shen et al., 2013; Yin et al., 1989, 1992), but later were linked to the Siberian Traps due to the temporal coincidence between these two events (Shen et al., 2012). Recent studies have focused on the spatial and the temporal distribution of the ash layers and their relationship to contemporaneous biotic and environmental changes (Xie et al., 2010; Shen et al., 2012, 2013).

3. Analytical techniques

3.1. Mineralogical and whole-rock compositions

Identification of bulk and clay minerals was carried out on unoriented powder mounts by X-ray diffraction (XRD) (BRUKER D8 ADVANGE in German) at the Guangzhou Institute of Geochemistry, Chinese Academy of Sciences (GIGCAS). Qualitative characterization and semi-quantitative characterization of mineralogy are based on peak intensity measurements on X-ray patterns. The diagnostic peak and the corrective intensity factor are indicated for each mineral. Semi-quantitative determination of the main clay species was based on the height of specific reflections, generally measured on ethylene glycol runs. The intensity of the 10 Å peak was taken as a reference, the other intensities were divided by a weight factor and all identified clay species values were summed to 100%. Corrective factors were determined by long-term empirical experiments at GIGCAS.

Whole-rock major elements were analyzed at the GIGCAS using wave-length X-ray fluorescence (XRF) spectrometry. A pre-ignition was used to determine the loss on ignition (LOI) prior to major element

analyses. Accuracy is within 1% for major elements. Whole-rock trace elements were analyzed using PerkinElmer Sciex ELAN 6000 Inductively Coupled Plasma-Mass Spectrometer (ICP-MS), following the techniques described by Liu et al. (1996). The USGS and Chinese National standards AGV-1, AGV-2, BHVO-2, GSR-1, GSR-2, GSR-3 and W-2 were chosen for calibrating element concentrations of the analyzed samples. Analytical uncertainties of REE and other incompatible element analyses are generally better than 5% (Supplementary Table 1).

3.2. Zircon U–Pb dating and Hf–O isotopic compositions

Zircon crystals were separated from ~3-kg crushed samples using conventional magnetic and density separation techniques and purified by hand-picking under a binocular microscope. All zircons were documented with transmitted and reflected light micrographs, as well as cathodoluminescence (CL) images to reveal the external and internal structures prior to U–Pb dating and Hf and O isotopic analyses and to choose potential target sites. The mount was vacuum-coated with high-purity gold prior to SIMS U–Pb and O isotopic analyses.

Measurements of U, Th and Pb isotopes and O isotopes were conducted using the Cameca IMS-1280 SIMS at the Institute of Geology and Geophysics, Chinese Academy of Sciences (IGGCAS). Analytical procedures for U–Pb dating are the same as those described by Li et al. (2009). After U–Pb dating, the sample mounts were re-ground for ~5 μm to ensure that any oxygen implanted in the zircon surface from the O_2^- beam used for U–Pb analysis is completely removed. Some grains have obtained CA-TIMS U–Pb ages in previous work (Shen et al., 2011). Analytical procedures are similar to those reported by Li et al. (2009).

In-situ zircon Lu–Hf isotopic analyses were carried out on a Neptune multi-collector ICP-MS equipped with a Geolas-193 laser-ablation system (LA-MC-ICPMS) at the IGGCAS. Lu–Hf isotopic analyses were obtained on the same zircon grains that were previously analyzed for U–Pb and O isotope. The detailed analytical technique and data correction procedures are described by Wu et al. (2006).

4. Results

4.1. Mineral compositions

Eleven PTB samples were selected for XRD analyses and the results are listed in Supplementary Table 2. The samples are mainly composed of a mixture of clay minerals including mixed-layer illite and smectite (47.3–93.3%), quartz (3.2–21.9%), feldspar (1.3–22.9%) and minor anatase and pyrite.

4.2. Whole-rock major and trace elements

The samples of the PTB volcanic ashes have high LOI contents (8–16%) (Table 1), consistent with the presence of large amounts of clay minerals. The samples have 16.5–28.2% Al_2O_3, 2.0–5.9% K_2O and 46–58% SiO_2 (Table 1). By using weight fractions of major oxides, the chemical index of alternation (CIA = $Al_2O_3/(Al_2O_3 + CaO^* + Na_2O + K_2O)$; Nesbitt and Young, 1982) and the chemical index of weathering (CIW = $Al_2O_3/(Al_2O_3 + CaO + Na_2O)$; Harnois, 1988) were calculated. The CIA and CIW values of the PTB volcanic ashes in South China are 77–86 and 63–96, respectively, indicating that all the samples have experienced intensive alteration and weathering. The Al_2O_3/TiO_2 of the PTB volcanic ashes are 22–151, similar to those reported by Zhou and Kyte (1988).

Total rare earth element (REE) concentrations of the samples vary from 135 to 603 ppm (Table 1). All the samples show negative Eu anomalies ($\delta Eu = 0.36$ to 0.57; $\delta Eu = Eu_{CN}/(Sm_{CN} + Gd_{CN})^{1/2}$, the subscript CN denotes chondrite-normalized; normalization values are after Sun and McDonough (1989)) on chondrite-normalized REE

diagrams (Fig. 4a) and pronounced negative Nb, Ta and Ti anomalies in their primitive mantle-normalized trace element patterns (Fig. 4b).

4.3. Zircon U–Pb ages and Hf–O isotopic compositions

The SIMS U–Pb ages for the zircon crystals from four samples (MS-A-25, MS-A-28, SS-24 and DP10-5-13) in the Meishan A, Shangsi and Dongpan sections are listed in Supplementary Table 3. The zircons display well-developed tetragonal dipyramids and magmatic zoning, none of them has core–rim structure. They have 36–775 ppm U and 18–488 ppm Th with Th/U of 0.36 to 2.11, which, together with the external morphology, is suggestive of a magmatic origin (Hoskin and Schaltegger, 2003). The weighted mean $^{206}Pb/^{238}U$ ages of the four samples are 252.2 ± 1.0 Ma (1σ, MSWD = 1.3), 251.7 ± 1.0 Ma (MSWD = 0.2), 253.5 ± 1.2 Ma (MSWD = 0.58) and 249.0 ± 0.82 Ma (MSWD = 0.75), respectively (Fig. 5). The ages are interpreted to be the crystallization age of the source materials.

Six samples from the Meishan, Shangsi, Chaotian and Dongpan sections were selected for Hf isotopic analyses, and five of them were selected for O isotopic analyses. The results are listed in Supplementary Tables 4 and 5. Zircons from the Meishan section have high $\delta^{18}O$ values (6.8 to 9.1‰), and negative $\varepsilon_{Hf(t)}$ values (−12.1 to −2.7) and the Hf two-stage model ages range from 1.45 to 2.04 Ga (Fig. 6 and Supplementary Table 4). Similar results are observed for zircons from other sections ($\delta^{18}O$ = 6.9 to 10.9‰, $\varepsilon_{Hf(t)}$ = −12.9 to −2.0, Hf two-stage model ages = 1.4 to 2.1 Ga) (Supplementary Table 4).

5. Discussion

5.1. The PTB volcanic ash layers and biological context

5.1.1. Temporal coincidence between the ash layer and the main extinction horizon

In the GSSP Meishan section, the decline of bio-diversity started in the limestone of the uppermost Permian, whereas the most dramatic decline occurred at the base of Bed 25 and at the base of Bed 28 (Song et al., 2013; Fig. 1). Consequently, the volcanic ash layers of Beds 25 and 28 are considered as the main extinction horizon (MEH) of the latest Permian and the second-order extinction (SOE) of the earliest Triassic, respectively (Song et al., 2013; Yin et al., 2007, 2012). The severest bio-decline is coincident with the most intense volcanism (Figs. 1 and 7). Irrespective of the exact ages of the volcanic ash, this can be taken as the direct evidence for the temporal coincidence between the PTB volcanism and the mass extinction event.

5.1.2. Volcanic intensity variation with biological context

Before making interpretations on apparent age coincidence, we once again need to assess the intensity of the PTB volcanism with particular reference to the frequent felsic ash fall events in the Late Permian. Taking the Shangsi section as an example, the duration of the volcanism that deposited the PTB volcanic ash (Mundil et al., 2004; Shen et al., 2011), in combination with the thickness of the ash layers, can be used to delineate the temporal variation in volcanic intensity (Fig. 7a). The Late Permian volcanism in the Shangsi section started at 254.8 Ma, and progressively reached its climax in the latest Permian, then declined gradually above the PTB, and ended at ~251.8 Ma. Similar temporal variations in volcanic intensity are observed in the Changsingian sections in the Meishan, Chaotian, Rencunping and Dongpan regions (Fig. 7b), assuming the same sedimentation rate for each section during Lopingian. We consider that the variation of the intensity of the late Permian volcanism may indicate a causal link between volcanic intensity and biological evolution.

Table 1
Major and trace elements of the PTB volcanic ashes in South China.

	MS-A-25	MS-A-28	CT-60	CT-61	SS-24	SS-25	DP10-2-16	DP10-5-13	RCP-10	RCP-11	RCP-12
Major elements											
SiO_2	50.88	57.85	50.10	46.14	45.96	52.10	53.78	53.02	51.01	53.11	51.03
TiO_2	0.45	0.74	0.45	0.44	0.25	0.49	0.31	0.74	0.51	0.17	0.54
Al_2O_3	26.36	16.45	25.13	24.05	19.15	23.94	24.34	28.22	25.90	26.11	26.57
Fe_2O_3	3.07	5.05	2.49	2.56	1.83	2.21	3.98	0.95	3.09	1.91	2.16
MgO	3.31	2.54	1.59	2.31	2.76	3.52	2.45	2.52	3.15	2.92	3.14
MnO	0.00	0.03	0.01	0.02	0.02	0.02	0.00	0.03	0.00	0.02	0.01
CaO	0.94	4.41	4.26	6.31	11.06	2.69	1.54	0.64	0.92	0.78	0.97
Na_2O	0.07	0.19	1.12	0.28	0.41	0.07	1.43	0.18	0.37	0.72	0.23
K_2O	5.23	4.46	4.13	4.67	2.82	3.65	2.01	5.85	5.49	5.65	5.79
P_2O_5	0.10	0.06	0.40	0.18	0.07	0.11	0.11	0.02	0.05	0.05	0.10
LOI	9.91	8.49	10.19	12.57	16.05	10.57	10.28	8.16	9.33	8.12	9.19
Total	100.31	100.27	99.87	99.53	100.38	99.36	100.28	100.33	99.82	99.57	99.73
Trace elements											
Sc	17.49	12.86	3.38	12.32	8.37	9.38	7.53	14.17	18.58	14.56	14.64
V	17.15	84.78	65.45	51.04	46.71	15.90	17.32	35.50	27.20	84.56	20.53
Cr	1.27	72.69	16.43	10.86	31.90	17.95	19.04	12.22	9.62	13.51	10.29
Co	0.60	9.68	10.99	16.80	7.13	2.39	5.95	10.37	2.59	4.33	2.75
Ni	4.79	26.50	27.54	34.58	16.80	23.93	28.56	39.32	11.06	36.56	21.51
Cu	9.35	25.00	44.61	93.89	40.72	5.29	63.13	18.57	18.16	12.72	7.97
Zn	138.20	44.72	68.26	71.99	29.03	46.48	81.71	60.46	147.50	77.47	48.90
Ga	31.31	21.61	23.25	26.97	7.12	9.09	25.97	31.63	31.28	28.15	34.28
Ge	1.13	1.55	0.64	1.11	0.65	0.96	1.53	1.44	1.37	1.37	1.77
Rb	106.40	146.50	128.10	157.50	55.01	72.86	90.28	173.00	151.20	168.90	180.10
Sr	168.90	212.20	972.20	644.50	447.70	75.99	129.70	54.06	40.59	50.43	42.74
Y	51.22	26.14	25.22	63.85	24.90	37.16	26.45	95.31	57.56	26.03	80.75
Zr	341.70	181.50	287.10	484.30	183.30	436.90	209.50	441.20	467.30	174.10	600.10
Nb	21.24	18.59	10.58	10.76	5.64	15.20	14.10	27.58	18.94	8.27	21.91
Cs	31.83	12.32	7.98	10.02	5.28	5.50	10.97	21.67	12.60	10.70	11.29
Ba	116.00	306.10	76.05	54.20	60.04	26.28	467.80	325.20	173.10	149.40	161.50
La	82.13	34.86	77.47	102.30	26.97	56.50	73.75	79.18	70.36	27.21	99.37
Ce	174.40	66.84	157.30	210.90	54.56	124.70	146.00	165.20	229.40	76.13	285.60
Pr	22.89	7.07	18.85	25.78	6.44	13.96	18.29	20.89	25.53	8.47	28.99
Nd	78.39	24.18	62.10	86.08	23.55	50.39	69.70	73.37	102.70	30.47	103.80
Sm	14.50	4.41	10.78	16.22	5.00	9.95	13.73	14.44	23.06	6.20	20.19
Eu	1.60	0.80	1.43	1.93	0.63	1.16	1.90	2.46	2.88	0.93	2.73
Gd	11.64	4.01	7.57	14.26	4.94	8.68	10.32	13.74	16.19	4.89	16.44
Tb	1.87	0.66	1.14	2.26	0.83	1.40	1.27	2.56	2.35	0.83	2.80
Dy	10.66	4.23	6.02	12.14	4.90	8.38	5.74	16.69	13.03	5.10	17.05
Ho	2.06	0.93	1.12	2.39	0.98	1.64	0.92	3.50	2.59	1.08	3.58
Er	5.64	2.83	2.85	6.14	2.77	4.48	2.33	10.37	7.12	3.23	10.12
Tm	0.78	0.43	0.44	0.87	0.40	0.63	0.32	1.52	1.02	0.52	1.52
Yb	4.72	2.68	2.76	5.26	2.50	3.81	2.00	9.22	6.27	3.45	9.57
Lu	0.67	0.41	0.38	0.77	0.38	0.53	0.30	1.32	0.92	0.53	1.45
Hf	14.98	4.92	8.52	13.68	7.02	12.74	6.39	18.93	17.61	8.32	20.38
Ta	2.75	1.13	2.15	2.75	1.48	2.14	2.22	2.67	2.91	2.27	3.33
Pb	27.11	24.90	35.11	42.49	19.91	36.32	21.21	13.65	20.29	34.46	21.08
Th	61.29	14.95	45.94	60.07	27.04	38.00	33.37	53.79	60.62	42.43	61.25
U	6.76	3.33	9.02	12.68	3.17	8.42	7.65	12.26	11.41	8.59	14.98
δEu	0.36	0.57	0.46	0.38	0.38	0.37	0.47	0.53	0.43	0.50	0.44
$\sum$REE	411.94	154.32	350.20	487.30	134.84	286.21	346.57	414.46	503.41	169.03	603.21

Note: $\delta Eu = Eu_{CN} / (Sm_{CN} + Gd_{CN})^{1/2}$, the subscript CN denotes chondrite-normalized, normalization values are after Sun and McDonough (1989).
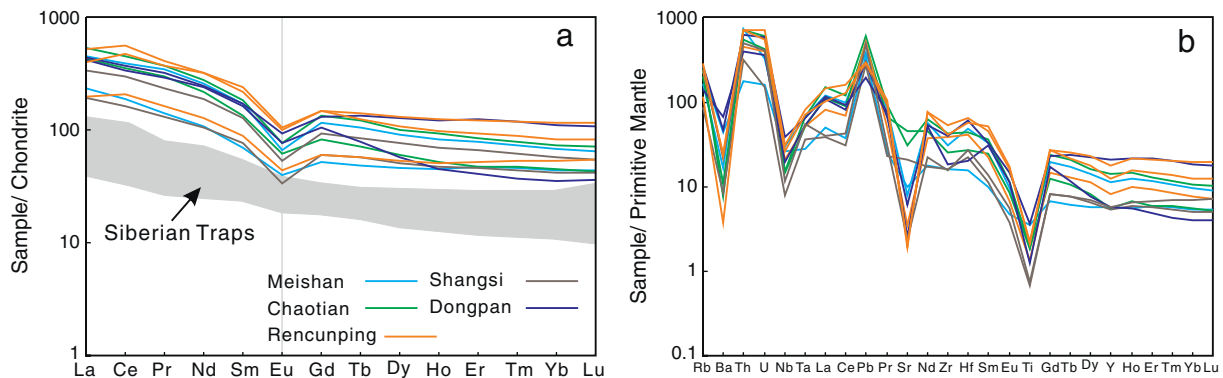

Fig. 4. (a) Chondrite-normalized REE patterns and (b) primitive mantle-normalized trace element patterns of the PTB volcanic ashes in South China. Chondrite and PM normalizing values from Sun and McDonough (1989).
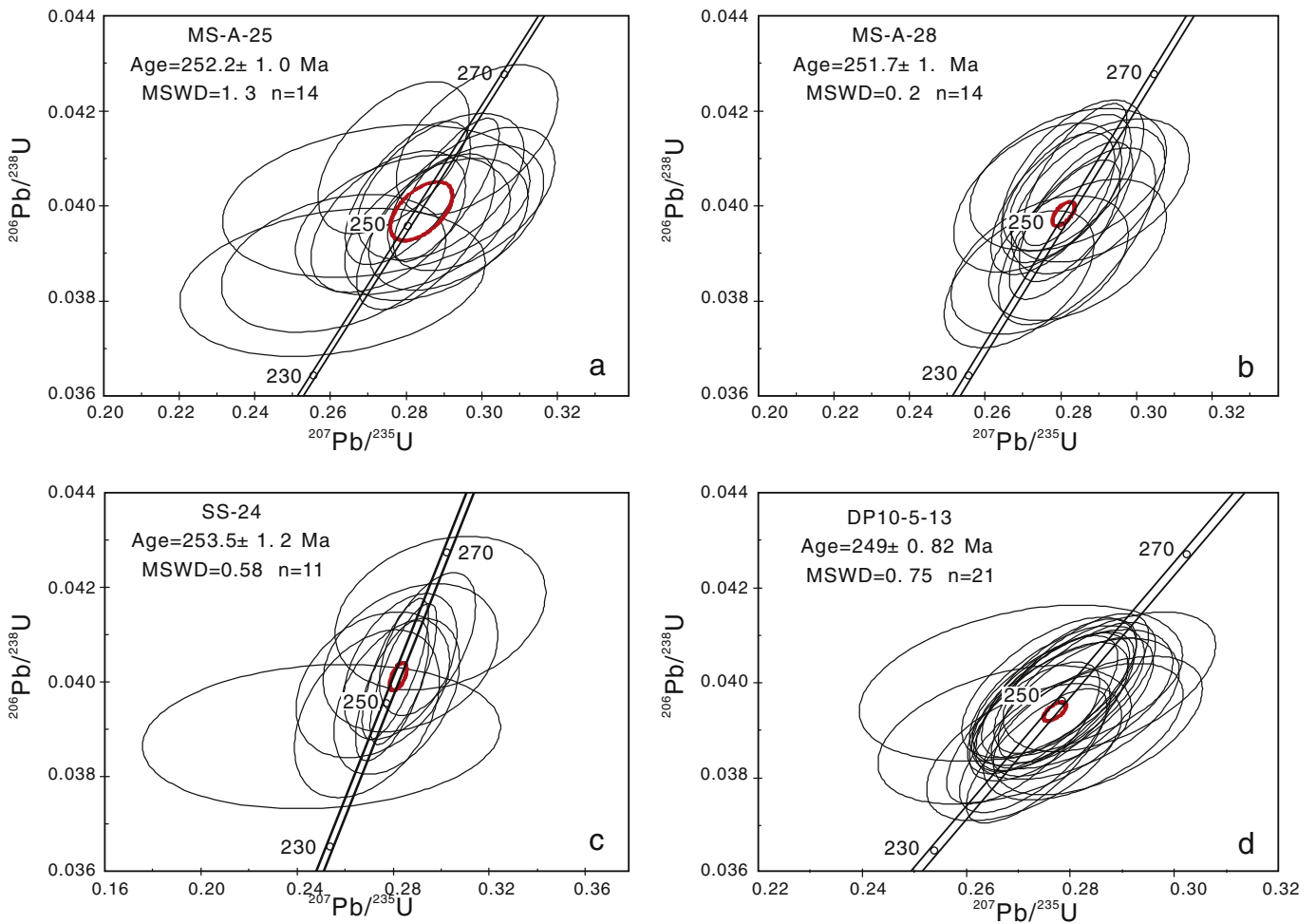
Fig. 5. U–Pb concordia diagrams for (a) MS-A-25, (b) MS-A-28, (c) SS-24, and (d) DP10-5-13.

5.2. Compositions of the PTB volcanic ashes in South China

The PTB volcanic ash layers in South China have Al_2O_3/TiO_2 of 22 to 151 with an average of 62. They are enriched in Cs, Zr, Hf, Ta and Th and depleted in Cr and Co (Table 1). They have negative Eu anomalies with δEu of 0.36 to 0.57 and an average value of 0.45. The PTB volcanic ashes classify as felsic on the Zr versus Ti, Al_2O_3 versus TiO_2 and Nb/Y versus Zr/TiO_2 diagrams (Fig. 8).

The PTB volcanic ashes have REE patterns identical to those of felsic volcanic rocks derived from volcanic arcs (Fig. 4a), indicating that the volcanic ash may have formed along a continental-plate margin during collision. On the basis of tectonomagmatic discrimination diagrams (Figs. 4 and 8), it is possible that the PTB volcanic ashes in South China record a transformation from calc-alkaline to peraluminous source rocks, consistent with a model of progressively evolving magmatism during the closure of the Paleo-Tethys.
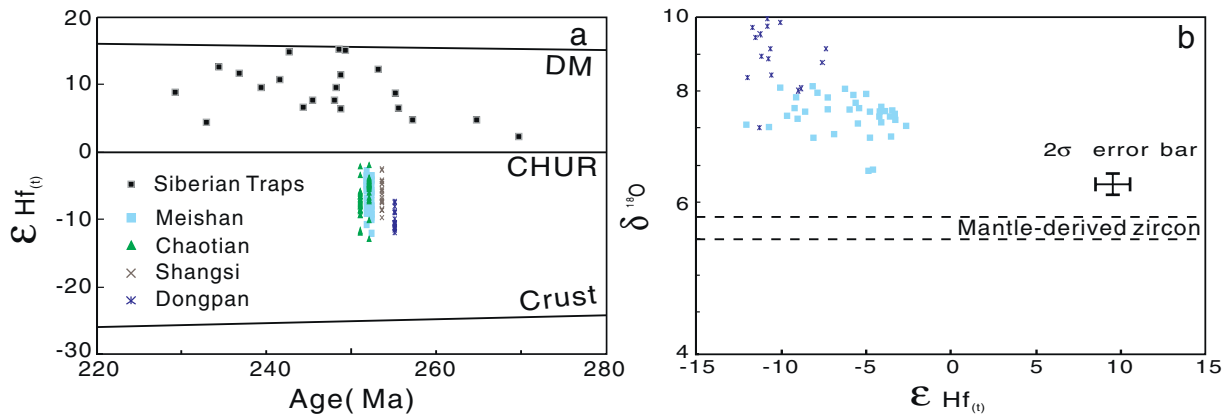

Fig. 6. (a) Plots of $\varepsilon_{Hf(t)}$ values versus U–Pb ages of the zircon grains from the PTB volcanic ashes in South China, and (b) $\varepsilon_{Hf(t)}$ versus $\delta^{18}O$ for zircons. Data for the Siberian Traps are compiled from Malitch et al. (2010).
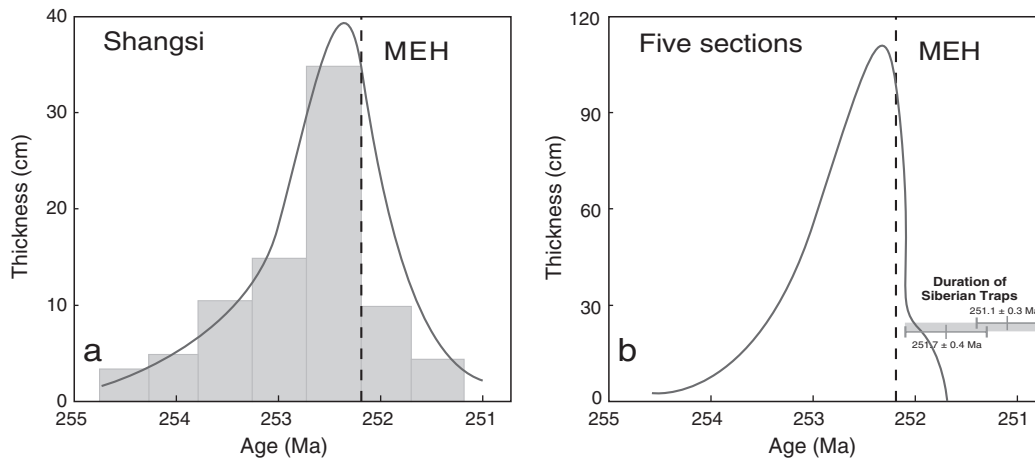
Fig. 7. A temporal variation in thickness of the PTB ash layers. (a) Shangsi section, and (b) five sections in South China. MEH = main extinction horizon; the isotopic dating data are after Shen et al. (2011) and Kamo et al. (2003).

The zircon grains from the PTB volcanic ashes have $\delta^{18}O$ values (6.8 to 10.9‰) higher than the mantle value (5.3 ± 0.3‰; Valley et al., 1998) and negative $\varepsilon_{Hf(t)}$ values (−12.9 to −2.0), consistent with a crustal origin. The Hf two-stage model ages of the zircons (1.4 to 2.1 Ga) further suggest that the PTB volcanic ash in South China was likely derived from melting of the Proterozoic basement.

5.3. Source and tectonic background of the PTB volcanic ashes in South China

The source rocks of the MEH and the PTB volcanic ashes have been proposed to be the Siberian Traps (e.g., Shen et al., 2012; Xu et al., 2007), or the volcanic rocks related to convergent plate tectonics in the western Panthalassa margin and Gondwana (Gao et al., 2013; Yin et al., 1989, 2007). The Siberian Traps hypothesis is problematic in that the Traps are mainly composed of mafic basalts, with tuff in the lowermost parts and minor felsic extrusives at the upper part, whereas the PTB volcanic ashes are felsic in composition. In addition, negative $\varepsilon_{Hf(t)}$ and high $\delta^{18}O$ isotope values of the zircons from the PTB volcanic ashes are consistent with a crustal origin, but at odds with the mantle origin of the Siberian Traps. Moreover, the oldest age of the Siberian Traps (251.7 Ma, Kamo et al., 2003) is younger than that of the MEH ashes at Meishan GSSP section (252.28 Ma, Shen et al., 2011). Rigorous comparison of zircon U–Pb ages between two laboratories shows that the youngest sequence of the Siberian Traps is ~300–500 Kyr younger than the major pulse of the PTB biotic extinction (Kamo et al., 2006). The whole duration of the PTB volcanic ash event in South China is 254.3 to 251.3 Ma (Bowring et al., 1998; Galfetti et al., 2007; Mundil et al., 2004; Shen et al., 2011), indicating that the 251.7–251.2 Ma flood basalts of the Siberian Traps are unlikely to be the source of the PTB volcanic ash.

While the genetic link of the PTB volcanic ash with the Siberian Traps can be ruled out, the exact source of the ash is difficult to determine. Spatial variation in the thickness and numbers of the PTB ash layers in South China (Fig. 3a) likely indicates that they may have originated from the west part of South China, where a Permian–Triassic continental magmatic arc (including gigantic intrusions and volcanics such as ignimbrite) is well documented east of Kunlun mountain. This continental magmatic arc was located in the Paleo-Tethys during Permian–Triassic transition (Gu et al., 1996; Guo et al., 1998; Ni, 2010). Zircons from the ignimbrites in the Hongshishan and Wubalebei regions are dated at 251.8 ± 2.3 Ma and 248.8 ± 1.7 Ma, respectively (Ni, 2010). Granodiorites in the Halagatu and Chulutaohai regions are dated at 255 ± 3.6 Ma (Sun et al., 2009) and 256.0 ± 9.6 Ma (Guo et al., 1998), respectively. In addition, Hf model ages (1.0–1.8 Ga) of the basement

underlain the East Kunlun magmatic arcs (Ni, 2010), are in agreement with the Hf model ages for the PTB volcanic ash in South China.

A review of large volcanic ash events in the history of the Earth can help elucidate the tectonic setting of the PTB volcanic ashes. For example, Ordovician volcanic ashes in the eastern North America and Western Europe represent one of the largest eruptions in Phanerozoic. This eruption produced a total of 1140 km³ of dense-rock-equivalent with dispersal over several million square kilometers (Huff et al., 1992). Most of the voluminous silicic rocks associated with ignimbrite flare-up eruptions display high $(^{87}Sr/^{86}Sr)_i$ with an average of 0.7075 and negative ε_{Nd} values (Ducea and Barton, 2007), consistent with significant involvement of continental crust in arc magmatism. This contrasts with the dominant mantle signature in flood volcanic episodes or in *steady-state* arc magmatism where basaltic triggers account for the low $(^{87}Sr/^{86}Sr)_i$ and high ε_{Nd} values. Toba Tuffs in Sumatra, Indonesia, which are the largest eruption in Quaternary, cover an area of at least 4,000,000 km² and erupted ~2500 km³ dense-rock-equivalent of ignimbrite (Chesner, 2012). The Toba Tuffs were considered to have formed in a destructive plate margin at fast subduction rate (Chesner, 2012). Their high initial $^{86}Sr/^{87}Sr$ of 0.71355–0.71502 and high $\delta^{18}O$ values (+8.7 to +10.3‰) (Chesner, 2012) are similar to those of the PTB volcanic ashes in South China.

Ignimbrite flare-up, in contrast to normal continental magmatic arc, may produce massive magmas in several millions or a few tens of millions of years. For example, 80–90% of the arc magmatic additions occur within a period of 10–15 Myr in North American continental arc (Ducea and Barton, 2007). The PTB volcanic ashes cover an area of >1,000,000 km² in South China, and possibly elsewhere in the Tethys region (Yin et al., 1992). However, the original extent of the volcanic ashes remains unknown because the PTB in most regions in the world is an unconformity (Yang et al., 1991). The extent of ignimbrite flare-up at PTB in the Paleo-Tethys may be much larger than what we estimated from the records of the PTB volcanic ashes in South China. Ignimbrite flare-up is considered to have been formed at continental magmatic arc at high convergence rates, where a relatively thick, old continental crust experienced regional shortening (de Silva and Gosnold, 2007; Hughes and Mahood, 2008). Paleomagnetic analysis shows that the southern margins of the Paleo-Tethys, Cimmerian continent such as the Qingtang, Sibumasu and Baoshan blocks and Indochina drift rapidly northwards in the Late Permian to Early Triassic, indicating a sudden, rapid convergence rate of the Paleo-Tethy during the Permian–Triassic transition (Li et al., 2004). Paleogeographic reconstruction also shows that the Paleo-Tethys was closed by the Indosinian orogenesis at the Early Triassic (~240 Ma, Li et al., 2004). Given the compositions of the PTB volcanic ashes and the rapid convergence rate
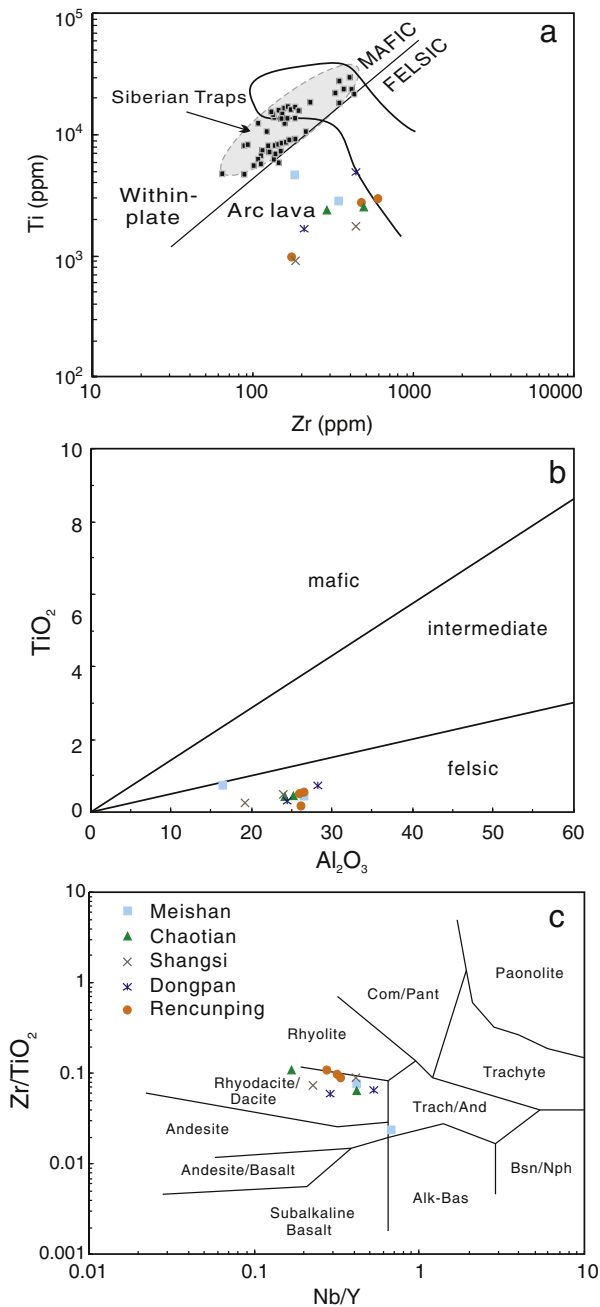
Fig. 8. (a) Zr versus Ti diagram (after Pearce (1982)), (b) plots of TiO_2 and Al_2O_3, and (c) Zr/TiO_2 versus Nb/Y diagram.

during the P–T transition, we tentatively suggest that the PTB volcanic ashes in South China are part of ignimbrite flare-up products derived from continental magmatic arc related to rapid subduction during the assemblage of Pangea.

5.4. Triggers of the PTB mass extinction: ignimbrite flare-up of Paleo-Tethys?

Potential cause of the PTB mass extinction has been debated on (1) bolide impacts (Becker et al., 2010; Becker et al., 2004; Kaiho et al., 2006; Retallack and Jahren, 2008); (2) rapid anoxia in deep water (e.g., Wignall and Twitchett, 1996, 2002); (3) a major sea-level fall or regression (Kozur, 2007); (4) large-scale continental flood volcanism (Campbell et al., 1992; Racki and Wignall, 2005; Renne et al., 1995) and (5) regional acidic volcanism of South China (Isozaki et al.,

2007; Xie et al., 2010; Yin et al., 1989). The bolide impact model is not favored, given the absences of Ir anomaly, shock mineral assemblage and meteor crater around PTB sections in the world, and prolonged two-episode mass extinction pattern (Song et al., 2013; Xie et al., 2005; Yin et al., 2007, 2012). There are evidences for sea-level changes and super-anoxia across the PTB, but whether they are ultimate causes for mass extinction or by-product of large-scale volcanism (Isozaki et al., 2004) remains unclear.

The Siberian Traps is widely believed as the trigger of the PTB mass extinction. However, high-resolution geochronological and detailed paleontological studies show that the Siberian Traps may postdate to the MEH of the PTB. The role of the Siberian Traps could be negated because the PTB volcanic ashes are felsic and crustally-derived but show no compositional affinity to mantle-derived flood basalts in the Siberian Traps. However, the Siberian flood volcanism may have caused the substantial increase of the temperature the sea-water across PTB (above the MEH) (Fig. 1) as documented by the oxygen isotopes of the conodonts in South China (Joachimski et al., 2012). The rise of temperature in sea water is similar to the global warming due to the Deccan Trap eruption (Keller et al., 2011; Li and Keller, 1998;) and the Emeishan LIP eruption (Chen et al., 2012). However, the global warming began *after* the MEH (Joachimski et al., 2012) (Fig. 1), thus ruling out the possibility of the Siberian Traps as the cause of the main extinction event of PTB.

The direct temporal coincidence of the PTB volcanic ashes and MEH and volcanic intensity cognation with biological context (Fig. 7) collectively highlight the role of volcanism on the PTB mass extinction event. A few recent studies documented the spatio-temporal distribution of the PTB ash layers and their relationship to contemporaneous biotic and environmental changes (Gao et al., 2013; Shen et al., 2012, 2013; Xie et al., 2010). Particularly, a close relationship between PTB volcanic ashes and carbon cycle perturbations during the P–T transition in the Xiakou and Xinmin sections is examined by Shen et al. (2012). These studies indicate that the PTB volcanism in South China have profound influences on biotic and environmental changes during the P–T transition. Thus, we tentatively suggest the PTB volcanic ashes in South China or Paleo-Tethys ignimbrite flare-up the most likely trigger of the main extinction event at the Permo-Triassic interval.

The PTB mass extinction pattern is the key for the understanding of its trigger. Two-pulse or -stage patterns of the extinction were documented by a number of studies (e.g., Song et al., 2013; Xie et al., 2005, 2007; Xie et al., 2010; Yin et al., 2007, 2012). The first pulse of extinction happened at MEH, and is denoted as the main extinction event or the Latest Permian mass extinction, which was marked by the extinction of 57% of species. The first crisis started at Bed 24, peaked at Bed 25, and recovered immediately above the extinction horizon (Song et al., 2013). The ignimbrite flare-up scenario accords with timing and pattern of the main extinction event or first-pulse mass extinction. Anoxia is clearly related to the second-pulse extinction in the earliest Triassic. Marine temperature proxies indicate that the spread of anoxia coincided with severe global warming, a stressor expected to affect shallow rather than deep-water taxa and high latitude rather than low latitude organisms (Song et al., 2013). The first-pulse extinction was not followed by subsequent rapid radiation, indicating that the stressful conditions persisted at least into the Griesbachian Stage (Song et al., 2013). If the global warming in the Early Triassic is related to the Siberian Traps, the second-pulse of mass extinction may be caused by the Siberian Traps although actual killing mechanisms should be scrutinized in detail.

The Paleo-Tethys ignimbrite flare-up model suggests that the eruption of felsic volcanic ashes is a trigger for the main extinction event of the PTB mass extinction. Major ignimbrites have volumes of 10^2–10^4 km^3 in American Andes. Ultraplinian eruption columns and co-ignimbrite ash clouds are commonly tens of kilometers in height and can inject large volumes of volcanic ash into the stratosphere, where it could persist for years and distribute in a hemispherical or global scale (Cather et al., 2009). Ultraplinian-type eruptions of felsic volcanoes at multiple sites in swarm may have driven severe environmental changes

in the biosphere through volcanic hazards; e.g., toxic gas emissions, developing dust/aerosol screens in the stratosphere (blocking sunlight), and pouring acid rain. Their cascading effects on the environments, such as temperature drop, dim daylight, cessation of photosynthesis, and shortage in food, may have led to the decline in biodiversity both in the ocean and on land; i.e., a scenario called 'volcanic ash winter' (Isozaki, 2009). All the responsible mechanisms likely became effective by the global development of 'volcanic ash winter' conditions.

6. Conclusions

The stratigraphic coincidence between the PTB volcanic ashes and the mass extinction event highlights the catastrophic effect of acidic volcanism on the biological evolution on Earth. The PTB volcanic ashes have no genetic link to the Siberian Traps. Instead they may have been derived from ignimbrite flare-up due to rapid subduction in the assembly of the Pangea Supercontinent. The Paleo-Tethys ignimbrite flare-up may have triggered the main PTB extinction event, with a possible scenario described by a 'volcanic ash winter' model, whereas the Siberian Traps may have been responsible for the second-order extinction event and Early Triassic ecological evolution, as a consequence of the greenhouse effect.

Acknowledgments

Appendix A. Supplementary data

Supplementary data to this article can be found online at http://dx.doi.org/10.1016/j.lithos.2014.05.011.

References

Becker, L., Poreda, R.J., Basu, A.R., Pope, K.O., Harrison, T.M., Nicholson, C., Iasky, R., 2004. Bedout: a possible end-Permian impact crater offshore of northwestern Australia. Science 304, 1469–1476.

Becker, L., Poreda, R.J., Hunt, A.G., Bunch, T.E., Rampino, M., 2010. Impact event at the Permian-Triassic boundary: Evidence from extraterrestrial noble gases in fullerenes. Science 291 (5508), 1530–1533.

Bowring, S.A., Erwin, D.H., Jin, Y.G., Martin, M.W., Davidek, E., Wang, W., 1998. U/Pb zircon geochronology and tempo of the end-Permian mass extinction. Science 280, 1039–1045.

Campbell, I.H., Czamanske, G.K., Fedorenko, V.A., Hill, R.I., Stepanov, V., 1992. Synchronism of the Siberian Traps and the Permian–Triassic boundary. Science 258, 1760–1763.

Cather, S.M., Dunbar, N.W., McDowell, F.W., McIntosh, W.C., Scholle, P.A., 2009. Climate forcing by iron fertilization from repeated ignimbrite eruptions: The icehouse-silicic large igneous province (SLIP) hypothesis. Geosphere 5 (3), 315–324.

Chen, B., Joachimski, M.M., Shen, S.Z., Lambert, L.L., Lai, X.L., Wang, X.D., Chen, J., Yuan, D.X., 2012. Permian ice volume and palaeoclimate history: oxygen isotope proxies revisited. Gondwana Research 24, 77–89.

Chesner, C.A., 2012. The Toba caldera complex. Quaternary International 258, 5–18.

Clark, D.L., Wang, C.Y., Orth, C.J., 1986. Conodont survival and low iridium abundances across the Permian–Triassic boundary in South China. Science 233, 984–986.

Courtillot, V.E., 1994. Mass extinctions in the last 300 million years: one impact and seven flood basalts? Israel Journal of Earth Sciences 43, 255–266.

Courtillot, V.E., Renne, P.R., 2003. On the age of flood basalt events. Geoscience 335, 113–140.

de Silva, S.L., Gosnold, W.D., 2007. Episodic construction of batholiths: insights from the spatiotemporal development of an ignimbrite flare-up. Journal of Volcanology and Geothermal Research 167, 320–335.

Ducea, M.N., Barton, M.D., 2007. Igniting flare-up events in Cordilleran arcs. Geology 35, 1047–1050.

Erwin, D.H., 1994. The Permo-Triassic extinction. Nature 367, 231–236.

Galfetti, T., Bucher, H., Ovtcharova, M., Schaltegger, U., Brayard, A., Bruhwiler, T., Goudemand, N., Weissert, H., Hochuli, P.A., Cordey, F., Guodun, K., 2007. Timing of the Early Triassic carbon cycle perturbations inferred from new U–Pb ages

and ammonoid biochronozones. Earth and Planetary Science Letters 258, 593–604.

Gao, Q.L., Zhang, N., Xia, W.C., Feng, Q.L., Chen, Z.Q., Zheng, J.P., Griffin, W.L., O'Reilly, S.Y., Pearson, N.J., Wang, G.Q., Wu, S., Zhong, W.L., Sun, X.F., 2013. Origin of volcanic ash beds across the Permian–Triassic boundary, Daxiakou, South China: petrology and U–Pb age, trace elements and Hf-isotope composition of zircon. Chemical Geology 360, 41–53.

Gu, F.B., Wu, X.N., Jiang, C.Y., 1996. Assemblages and tectonic environment of the Variscan–Indosinian granitoid in the eastern Kunlun. Qinghai Geology 1, 18–36 (in Chinese with English abstract).

Guo, Z.F., Deng, J.F., Xu, Z.Q., Mo, X.X., Luo, Z.H., 1998. Late Palaeozoic–Mesozoic intracontinental orogenic process and intermediate-acidic igneous rocks from the eastern Kunlun Mountains of northwestern China. Geoscience 12, 344–352 (in Chinese with English abstract).

Harnois, L., 1988. The CIW index: a new chemical index of weathering. Sedimentary Geology 55, 319–322.

Hoskin, P.W.O., Schaltegger, U., 2003. The composition of zircon and igneous and metamorphic petrogenesis. In: Hanchar, J.M., Hoskin, P.W.O. (Eds.), Zircon. Reviews in Mineralogy and Geochemistry, 53, pp. 27–55.

Huff, W.D., Bergström, S.M., Kolata, D.R., 1992. Gigantic Ordovician volcanic ash fall in North America and Europe: biological, tectonomagmatic, and event-stratigraphic significance. Geology 20, 875–878.

Hughes, G.R., Mahood, G.A., 2008. Tectonic controls on the nature of large silicic calderas in volcanic arcs. Geology 36, 627–630.

Isozaki, Y., 2009. Integrated "plume winter" scenario for the double-phased extinction during the Paleozoic-Mesozoic transition: The G-LB and P-TB events from a Panthalassan perspective. Journal of Asian Earth Sciences 36 (6), 459–480.

Isozaki, Y., Yao, J.X., Matsuda, T., Sakai, H., Ji, Z.S., Shimizu, N., Kobayashi, N., Kawahata, H., Nishi, H., Takano, M., Kubo, T., 2004. Stratigraphy of the Middle–Upper Permian and Lowermost Triassic at Chaotian, Sichuan, China — record of Late Permian double mass extinction event. Proceedings of the Japan Academy Series B-Physical and Biological Sciences 80, 10–16.

Isozaki, Y., Shimizu, N., Yao, J.X., Ji, Z.S., Matsuda, T., 2007. End-Permian extinction and volcanism-induced environmental stress Permian–Triassic boundary interval of a lower-slope facies at Chaotian, South China. Paleogeography, Paleoclimatology, Paleoecology 252, 39–55.

Joachimski, M.M., Lai, X.L., Shen, S.Z., Jiang, H.S., Luo, G.M., Chen, B., Chen, J., Sun, Y.D., 2012. Climate warming in the latest Permian and the Permian–Triassic mass extinction. Geology 40, 195–198.

Kaiho, K., Kajiwara, Y., Chen, Z.Q., Gorjan, P., 2006. A sulfur isotope event at the end of the Permian. Chemical Geology 235, 33–47.

Kamo, S.L., Czamanske, G.K., Amelin, Y., Fedorenko, V.A., Davis, D.W., Trofimov, V.R., 2003. Rapid eruption of Siberian flood-volcanic rocks and evidence for coincidence with the Permian–Triassic boundary and mass extinction at 251 Ma. Earth and Planetary Science Letters 214, 75–91.

Kamo, S.L., Crowley, J., Bowring, S.A., 2006. The Permian–Triassic boundary event and eruption of the Siberian flood basalts: an inter-laboratory U–Pb dating study. Geochimica et Cosmochimica Acta 7018, A303.

Keller, G., Bhowmick, P.K., Upadhyay, H., Dave, A., Reddy, A.N., Jaiprakash, B.C., Adatte, T., 2011. Deccan volcanism linked to the Cretaceous-Tertiary boundary mass extinction: New evidence from ONGC Wells in the Krishna-Godavari Basin. Journal of the Geological Society of India 78 (5), 399–428.

Kozur, H.W., 2007. Biostratigraphy and event stratigraphy in Iran around the Permian-Triassic Boundary (PTB): Implications for the causes of the PTB biotic crisis. Global and Planetary Change 55 (1–3), 155–176.

Li, L.Q., Keller, Q., 1998. Abrupt deep-sea warming at the end of the Cretaceous. Geology 26 (11), 995–998.

Li, P.W., Rui, G., Cui, J.W., Ye, G., 2004. Paleomagnetic analysis of eastern Tibet: implications for the collisional and amalgamation history of the Three Rivers Region, SW China. Journal of Asian Earth Sciences 24, 291–310.

Li, X.H., Li, W.X., Wang, X.C., Li, Q.L., Liu, Y., Tang, G.Q., 2009. Role of mantle-derived magma in genesis of early Yanshanian granites in the Nanling Range, South China: in situ zircon Hf–O isotopic constraints. Science in China Series D: Earth Sciences 52, 1262–1278.

Li, Z.S., Zhan, L.P., Zhu, X.F., Zhang, J.H., Jin, R.G., Liu, G.F., Sheng, H.B., Shen, G.M., Dai, J.Y., Huang, H.Q., Xie, L.C., Yan, Z., 1986. Mass extinction and geological events between Palaeozoic and Mesozoic era. Acta Geologica Sinica 1, 1–21 (in Chinese with English abstract).

Liu, Y., Liu, H.C., Li, X.H., 1996. Simultaneous and precise determination of 40 trace elements in rock samples using ICP-MS. Geochimica 25, 552–558 (in Chinese with English abstract).

Malitch, K.N., Belousova, E.A., Griffin, W.L., Badanina, I.Y., Pearson, N.J., Presnyakov, S.L., Tuganova, E.V., 2010. Magmatic evolution of the ultramafic–mafic Kharaelakh intrusion (Siberian Craton, Russia): insights from trace-element, U–Pb and Hf-isotope data on zircon. Contributions to Mineralogy and Petrology 159, 753–768.

Metcalfe, I., Nicoll, R.S., Black, L.P., Mundil, R., Renne, P., Jagodzinski, E.A., Chengyuan, Wang, 1999. Isotope geochronology of the Permian–Triassic boundary and mass extinction in South China. In: Hongfu, Yin, Jinnan, Tong (Eds.), Pangea and the Paleozoic–Mesozoic Transition. China University of Geosciences Press, Wuhan, pp. 134–137.

Mundil, R., Metcalfe, I., Ludwig, K.R., Renne, P.R., Oberli, F., Nicoll, R.S., 2001. Timing of the Permian–Triassic biotic crisis: implications from new zircon U/Pb age data and their limitations. Earth and Planetary Science Letters 187, 131–145.

Mundil, R., Ludwig, K.R., Metcalfe, I., Renne, P.R., 2004. Age and timing of the Permian mass extinctions: U/Pb dating of closed-system zircons. Science 305, 1760–1763.

Nesbitt, H., Young, G., 1982. Early Proterozoic climates and plate motions inferred from major element chemistry of lutites. Nature 299, 715–717.

Ni, J.Y., 2010. Zircon U–Pb Ages and Tectonic Setting of Permian–Triassic Volcanic Rocks in East Kunlun Orogenic Belt. (MS thesis) Chinese Academy of Geological Science, (65 p.).

Pearce, J.A., 1982. Trace element characteristics of lavas from destructive plate boundaries. In: Thorpe, R.S. (Ed.), Orogenic Andesites and Related Rocks, pp. 528–548.

Racki, G., Wignall, P.B., 2005. Late Permian double-phased mass extinction and volcanism: an oceanographic perspective. Developments in Palaeontology and Stratigraphy 20, 263–297.

Reichow, M.K., Saunders, A.D., White, R.V., Pringle, M.S., Al'Mukhamedov, A.I., Medvedev, A.I., Kirda, N.P., 2002. ^{40}Ar/^{39}Ar dates from the West Siberian Basin: Siberian flood basalt province doubled. Science 296, 1846–1849.

Renne, P.R., Zhang, Z.C., Richards, M.A., Black, M.T., Basu, A.R., 1995. Synchrony and causal relations between Permian–Triassic boundary crises and the Siberian flood volcanism. Science 269, 1413–1416.

Retallack, G.J., Jahren, A.H., 2008. Methane release from igneous intrusion of coal during Late Permian extinction events. Journal of Geology 116, 1–20.

Sadovnikov, G.N., 2008. On the global stratotype section and point of the Triassic base. Stratigraphy and Geological Correlation 16, 31–46.

Shen, S.Z., Crowley, J.L., Wang, Y., Bowring, S.A., Erwin, D.H., Sadler, P.M., Cao, C.Q., Rothman, D.H., Henderson, C.M., Ramezani, J., Zhang, H., Shen, Y.A., Wang, X.D., Wang, W., Mu, L., Li, W.Z., Tang, Y.G., Liu, X.L., Liu, L.J., Zeng, Y., Jiang, Y.F., Jin, Y.G., 2011. Calibrating the end-Permian Mass extinction. Science 334, 1367–1372.

Shen, J., Algeo, T.J., Hu, Q., Zhang, N., Zhou, L., Xia, W.C., Xie, S.C., Feng, Q.L., 2012. Negative C-isotope excursions at the Permian–Triassic boundary linked to volcanism. Geology 40, 963–966.

Shen, J., Algeo, T., Hu, Q., Xu, G., Zhou, L., Feng, Q., 2013. Volcanism in South China during the Late Permian and its relationship to marine ecosystem and environmental changes. Global and Planetary Change 105, 121–134.

Song, H.J., Wignall, P.B., Tong, J.N., Yin, H.F., 2013. Two pulses of extinction during the Permian–Triassic crisis. Nature Geoscience 6, 52–56.

Sun, S.S., McDonough, W.F., 1989. Chemical and isotopic systematics of oceanic basalts: implications for mantle composition and processes. In: Saunders, A.D., Norry, M.J. (Eds.), Magmatism in the Ocean Basins: Geological Society London Special Publications. 42, pp. 313–345.

Sun, Y., Pei, X.Z., Ding, S.P., Li, R.B., Feng, J.Y., Zhang, Y.F., Li, Z.C., Chen, Y.X., Zhang, X.F., Chen, G.C., 2009. Halagatu magma mixing granite in the east Kunlun Mountains: evidence from zircon U–Pb dating. Acta Geologica Sinica 83 (7), 1000–1010 (in Chinese with English abstract).

Valley, J.W., Kinny, P.D., Schulze, D.J., Spicuzza, M.J., 1998. Zircon megacrysts from kimberlite: oxygen isotope variability among mantle melts. Contributions to Mineralogy and Petrology 133 (1–2), 1–11.

Wignall, P.B., Twitchett, R.J., 1996. Oceanic anoxia and the end Permian mass extinction. Science 272 (5265), 1155–1158.

Wignall, P.B., Twitchett, R.J., 2002. Extent, duration, and nature of the Permian-Triassic superanoxic event. Geological Society of America (Special Paper) 356, 395–414.

Wu, F.Y., Yang, Y.H., Xie, L.W., Yang, J.H., Xu, P., 2006. Hf isotopic compositions of the standard zircons and baddeleyites used in U–Pb geochronology. Chemical Geology 234, 105–126.

Xie, S.C., Pancost, R.D., Yin, H.F., Wang, H.M., Evershed, R.P., 2005. Two episodes of microbial change coupled with Permo/Triassic faunal mass extinction. Nature 434, 494–497.

Xie, S.C., Pancost, R.D., Huang, J.H., Wignall, P.B., Yu, J.X., Tang, X.Y., Chen, L., Huang, X.Y., Lai, X.L., 2007. Changes in the global carbon cycle occurred as two episodes during the Permian Triassic crisis. Geology 35, 1083–1086.

Xie, S.C., Pancost, R.D., Wang, Y.B., Yang, H., Wignall, P.B., Luo, G.M., Jia, C.L., Chen, L., 2010. Cyanobacterial blooms tied to volcanism during the 5 m.y. Permo-Triassic biotic crisis. Geology 38 (5), 447–450.

Xu, L., Lin, Y.T., Shen, W.J., Qi, L., Xie, L.W., Ouyang, Z.Y., 2007. Platinum-group elements of the Meishan Permian–Triassic boundary section: evidence for flood basaltic volcanism. Chemical Geology 246, 55–64.

Yang, J.H., Cawood, P.A., Du, Y.S., Huang, H., Huang, H.W., Tao, P., 2012. Large igneous province and magmatic arc sourced Permian-Triassic volcanogenic sediments in China. Sedimentary Geology 261–262, 120–131.

Yang, Z.Y., Wu, S.B., Yin, H.F., Xu, Q.R., Zhang, K.X., 1991. Geological Events During the Permian–Triassic Transition of South China. Geological Publishing House, pp. 1–190.

Yin, H.F., Huang, S.J., Zhang, K.X., Yang, F.Q., Ding, M.H., Bi, X.M., Zhang, S.X., 1989. Volcanism at the Permian–Triassic Boundary in South China and its effects on mass extinction. Acta Geologica Sinica 63, 169–180 (in Chinese with English abstract).

Yin, H.F., Huang, S., Zhang, K.X., Hansen, H., Yang, F.Q., Ding, M., Bie, X., 1992. The effects of volcanism on the Permo-Triassic mass extinction in South China. In: Sweet, W.C., et al. (Eds.), Permo-Triassic Events in the Eastern Tethys. Cambridge University Press, Cambridge, pp. 169–174.

Yin, H.F., Zhang, K.X., Tong, J.N., Yang, Z.Y., Wu, S.B., 2001. The global stratotype section and point (GSSP) of the Permian–Triassic boundary. Episodes 242, 102–114.

Yin, H.F., Feng, Q.L., Lai, X.L., Baud, A., Tong, J.N., 2007. The protracted Permo-Triassic crisis and multi-episode extinction around the Permian–Triassic boundary. Global and Planetary Change 55, 1–20.

Yin, H.F., Xie, S.C., Luo, G.M., Algeo, T.J., Zhang, K.X., 2012. Two episodes of environmental change at the Permian–Triassic boundary of the GSSP section Meishan. Earth-Science Reviews 115, 163–172.

Zhou, L., Kyte, F.T., 1988. The Permian–Triassic boundary event — a geochemical study of three Chinese sections. Earth and Planetary Science Letters 904, 411–421.